Bioorganic Chemistry 90 (2019) 103108

Contents lists available at ScienceDirect

Bioorganic Chemistry

journal homepage: www.elsevier.com/locate/bioorg

Substituted phenyl[(5-benzyl-1,3,4-oxadiazol-2-yl)sulfanyl]acetates/acetamides as alkaline phosphatase inhibitors: Synthesis, computational studies, enzyme inhibitory kinetics and DNA binding studies

Zafar Iqbal[a], Zaman Ashraf[a,*], Mubashir Hassan[b], Qamar Abbas[c], Erum Jabeen[a]

[a] Department of Chemistry, Allama Iqbal Open University, Islamabad 44000, Pakistan
[b] Institute of Molecular Biology and Biotechnology, The University of Lahore, Pakistan
[c] Department of Physiology, University of Sindh, Jamshoro, Pakistan

ARTICLE INFO

Keywords:
Alkaline phosphatase inhibitors
Enzyme kinetics
DNA binding studies
Molecular docking

ABSTRACT

Substituted phenyl[(5-benzyl-1,3,4-oxadiazol-2-yl)sulfanyl]acetates/acetamides **9a-j** were synthesized as alkaline phosphatase inhibitors. Phenyl acetic acid **1** through a series of reactions was converted into 5-benzyl-1,3,4-oxadiazole-2-thione **4**. The intermediate oxadiazole **4** was then reacted with chloroacetyl derivatives of phenols **6a-f** and anilines derivatives **8a-d** to afford the title oxadiazole derivatives **9a-j**. All of the title compounds **9a-j** were evaluated for their inhibitory activity against human alkaline phosphatise (ALP). It was found that compounds **9a-j** exhibited good to excellent alkaline phosphatase inhibitory activity especially **9h** displayed potent activity with IC_{50} value 0.420 ± 0.012 μM while IC_{50} value of standard (KH_2PO_4) was 2.80 μM. The enzyme inhibitory kinetics of most potent inhibitor **9h** was determined by Line-weaever Burk plots showing non-competitive mode of binding with enzyme. Molecular docking studies were performed against alkaline phosphatase enzyme (1EW2) to check the binding affinity of the synthesized compounds **9a-j** against target protein. The compound **9h** exhibited excellent binding affinity having binding energy value (−7.90 kcal/mol) compared to other derivatives. The brine shrimp viability assay results proved that derivative **9h** was non-toxic at concentration used for enzyme assay. The lead compound **9h** showed LD_{50} 106.71 μM while the standard potassium dichromate showed LD_{50} 0.891 μM. The DNA binding interactions of the synthesized compound **9h** was also determined experimentally by spectrophotometric and electrochemical methods. The compound **9h** was found to bind with grooves of DNA as depicted by both UV–Vis spectroscopy and cyclic voltammetry with binding constant values 7.83×10^3 and $7.95 \times 10^3\ M^{-1}$ respectively revealing significant strength of **9h**-DNA complex. As dry lab and wet lab results concise each other it was concluded that synthesized compounds, especially compound **9h** may serve as lead compound to design most potent inhibitors of human ALP.

1. Introduction

Azoles are a class of compounds having five membered heterocyclic rings that contains one nitrogen atom and at least one other non carbon atom in the ring. The widespread use of azoles in medicinal chemistry have been reported and is being treated as privileged structured class exhibiting wide range of biological activities as antifungal, analgesic, hypolipidemic, ulcerogenic, anti tubercular, antiviral, antimicrobial, antineoplastic, anticancer, inhibition of tyrosinase, cathepsin K, anti-inflammatory, hypnotic, genotoxic, muscle anticonvulsant, lipid per oxidation inhibitor [1–4] and vasodilator. Some of the oxadiazole derivatives act as muscle relaxants, hypnotic, sedatives, and show anti-mitotic activities [5]. Azole heterocycles show strong hydrogen bonding interactions with the receptors that increase their pharmacological activity. The well-known examples of drugs having the azoles nucleus include nesapidil as antihypertensive, raltegravir as antiretroviral, furamizole as antibiotic drug and zibotenten as anticancer drug. Well known azole derivatives theophylline and pyrazole are widely used alkaline phosphatase inhibitors [6].

Alkaline phosphatase (ALP, E.C.3.1.3.1.) is a non-specific phosphomonoester hydrolase that catalyzes the hydrolysis and transphosphorylation of a wide variety of organic monophosphates and regulates the functions of many biological systems [7–9]. Cell regulation is an important biological process and is being controlled by phosphatase enzyme due to which phosphatase are the area of immense interest in the field of pharmaceutical research [10]. ALP has very complex

* Corresponding author.
E-mail address: mzchem@yahoo.com (Z. Ashraf).

https://doi.org/10.1016/j.bioorg.2019.103108
Received 18 May 2019; Received in revised form 1 July 2019; Accepted 2 July 2019
Available online 03 July 2019

structure both in human and *Escherichia coli*. Substrate specificity is an area of interest in research because there are different active sites in the substrates and dephosphorylation at particular site is very much important for the proper cellular functioning [11]. Tissue nonspecific alkaline phosphatase is articulated in developing spinal and brain which shows its physiological role in the development of CNS [12]. Proliferation and migration in CNS is also associated with TNAP. Wide spectrum of monoesters of phosphoric acid is being hydrolyzed by tissue nonspecific alkaline phosphatase [13]. If the level of alkaline phosphatase exceeds the reference range with in body it is termed as elevated alkaline phosphatase. Homeostasis within the body is being maintained by alkaline phosphatase [14]. Elevated level of ALP in body may result in a number of diseases as metabolic disorder, dysregulation in CNS, mineralization disorders and obesity, osteoblastic bone tumors, osteomalacia, osteoporosis, bone conditions, biliary obstruction, hepatitis, myelofibrosis, myocardial infarction, leukemoid reaction, lymphoma, sarcoidosis, hyperparathyroidism and hyperthyroidism are associated with elevated level of the alkaline phosphatase enzyme [15]. It is evident from literature that azoles represent imperative pharmacophores and have a wide range of therapeutic properties [16]. Keeping in view the importance of this moiety the present work describe the synthesis of substituted phenyl [(5-benzyl-1,3,4-oxadiazol-2-yl)sulfanyl]acetates/acetamide **9a-j** as alkaline phosphatase inhibitors. The computational studies and enzyme inhibitory kinetics was determined to compare the wet lab results with dry lab. The DNA binding studies was also determined to check its mode of binding with DNA which in turn helps us to predict its antiproliferative properties. The brine shrimp cytotoxicity test was also performed and Herein we selected 1,3,4-oxadiazole as alkaline phosphatase inhibitors due to their widespread use as therapeutic drugs.

2. Results and discussion

2.1. Synthesis

Methyl 2-phenylacetate **2** and 2-phenylacetohydrazide **3** were synthesized according to the already reported methods [17,18]. The Scheme **I** depicts the synthesis of oxadiazole **4** employing slight modifications in already reported method. FTIR spectrum confirmed the formation of oxadiazole compound **4** having peak at 1635 cm^{-1} indicated the presence of C═N absorption and SH at 2853 cm^{-1}. The chloroacetyl derivatives of phenols **6a-f** were synthesized by reacting substituted phenols **5a-f** with chloroacetyl chloride in the presence of triethyl amine as base. The anilines derivatives **8a-d** were obtained by reacting anilines **7a-d** with chloroacetyl chloride by following the same procedure used in the preparation of derivatives **6a-f**. The title compounds **9a-j** was obtained in good to excellent yield by reacting oxadiazole **4** with substituted phenol derivatives **6a-f** and aniline derivatives **8a-d**. This involves the alkylation of mercapto group of oxadiazole **4.** The formation of the final products was ascertained by FTIR, ^{1}H NMR and ^{13}C NMR spectroscopy.

2.2. Bioassay for alkaline phosphatase inhibitory activity

In the present work oxadiazole based derivatives **9a-j** were designed based upon our previous investigations. Oxadiazole based ALP inhibitors analogues have been designed to evaluate their inhibitory activity against ALP enzyme. The azole derivatives **9a-j** was synthesized by following the already reported method with slight modification shown in Scheme 1. New analogues **9a-j** has been synthesized by substituting hydrophilic and hydrophobic groups on phenyl ring in order to check ALP inhibitory activity. We have evaluated the role of floro, chloro, alkyl, acetyl, methoxy and aldehydic functional groups on benzene ring in order to check ALP inhibitory activity. KH_2PO4 a well known clinically used ALP inhibitor was used as reference drug for comparison purpose. The synthesized compounds **9h, 9b, 9c, 9i**, and **9a** showed good to excellent inhibition of ALP with IC_{50} ranged from 0.42 μM to 2.37 μM higher activities compared to standard KH_2PO_4 having IC_{50} 2.80 μM. Table 1 presented the IC_{50} values of the synthesized azole derivatives **9a-j** and it was observed that compound **9h** exhibited the most potent alkaline phosphatase inhibitory activity with IC_{50} 0.420 μM. The presence of the trifloromethyl moiety in compound **9h** might be playing very important role in the alkaline phosphatase inhibitory activity. The derivatives **9b** and **9c** possess methoxy and alkyl substitution respectively having IC_{50} 1.23 μM and showed activity lower than compound **9h** but higher than rest of the analogues. The compound **9i** possesses 4-bromo on phenyl ring having IC_{50} 1.79 μM showed excellent activity. Similarly compound **9a** in which phenyl ring was unsubstituted having IC_{50} 2.37 μM showed activity better than the standard KH_2PO4. The compound **9d, 9e, 9f, 9g** and **9j** having methylene 1,3-dioxal moiety, 4-allyl-2methoxy, 4-formyl-2-methoxy, phenyl and 4-chloro respectively showed less activity compared to other derivatives and as compared to standard. It has now been verified that these substitutions does not play any important role in alkaline phosphatase inhibitory activity. On the basis of these results we propose that derivative **9h** having trifloro methyl substituent may serve as a structural model for the design and development of novel ALP inhibitors.

2.3. Kinetic study

On the basis of IC_{50} value we selected the most potent inhibitor **9h** to understand the inhibitory mechanism of synthesized compound. The results were presented in Table 2 and Fig. 1. The kinetic studies showed inhibition mechanism of compound **9h** to be non-competitive inhibitor of calf IALP. The inhibition constant Ki (0.360) was determined from **fig B**. The value of 1/Vmax is increased to a new value while that of Km remain same which indicated that compound **9h** simply lowers the concentration of enzyme by a non-competitive binding mode (**Fig. A and B**).

2.4. Cytotoxicity studies

The viability assay of derivatives **9a-j** was carried out on brine shrimp in order to check the cytotoxicity of the synthesized compounds. The brine shrimp cytotoxicity results showed that synthesized compounds are no-toxic to the shrimps at concentration range 70– 125 μM. As higher is the LD_{50} values lower is the cytotoxicity and vice versa. LD_{50} values were calculated and are shown in Fig. 2 and the results showed that compound **9j** showed highest LD_{50} 125.29 μM and hence the least cytotoxicity. The lead compound **9h** also showed LD_{50} 106.71 μM and hence the much less cytotoxicity than the standard KH_2PO4. The concentration of compound **9h** selected for other bioassay is less than the LD_{50} value.

2.5. DFT calculations

The spatial characteristics, nodal patterns and involvement of individual atom in charge transfer process was assayed by computing their frontier molecular orbitals. The DFT calculations revealed that HOMO orbital as well as LUMO orbitals were solely spread over S-alkylated moiety of the molecule which revealed that this part of molecule will actively participate in any (oxidation or reduction) charge transfer process Fig. 3**.**

The molecular potential energy surface (MPES) was computed to define nucleophilic and electrophilic regions in the molecule. The Fig. 4 shows the computed MPES model at DFT/B3LYP/6-311G**(++). It is interesting to find that the nucleophilic character was dominating in the molecule as revealed by dominance of reddish shade in MPES. This is due to presence of pi-electron excessive oxadiazole ring and electron attracting -CF_3 group at side chain phenyl. It can be predicted that there is merely any probability of developing electrostatic interactions

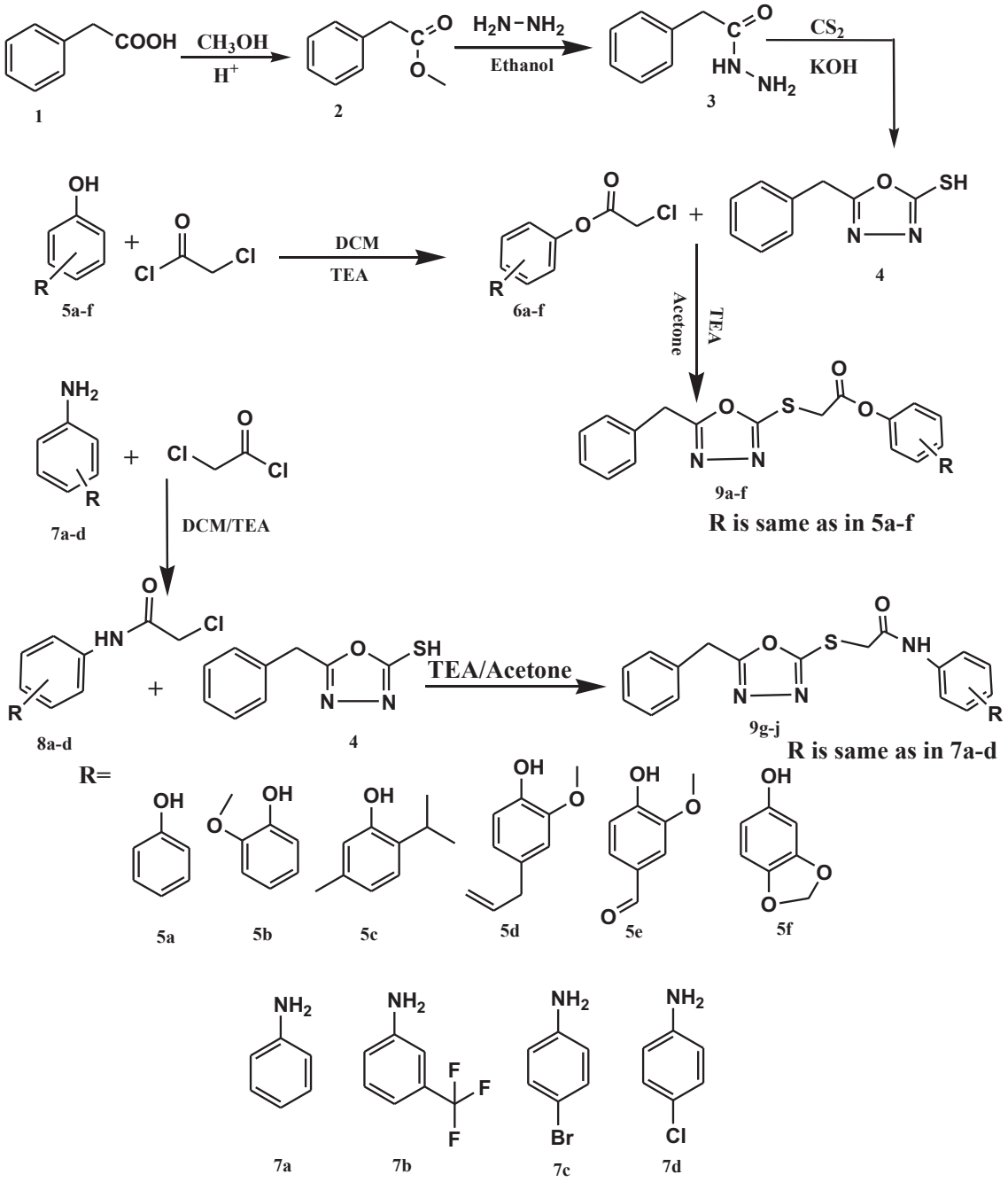

Scheme 1. Synthetic route for substituted phenyl[(5-benzyl-1,3,4-oxadiazol-2-yl)sulfanyl] acetates/acetamides **9a-j**.

between **9h** molecule and negatively charged phosphate backbone of DNA as **9h** is deficient in significant electrophilic character. Further, electronic charge spread over the molecule predicts that stacking of such electron rich structure between DNA base pairs may generate repulsion with π electron cloud of DNA base pairs. This may create hindrance to intercalation of **9h** through its planner part.

2.5.1. Mechanism of charge transfer process

The cyclic voltammograms of the **9h** exhibited reversible redox peak with oxidation at 0.389 V and reduction peak at 0.314 V at 100 mV/s Fig. 5. The Ep_a-Ep_c was > 60 mV which revealed that the oxidation and reduction peaks does not correspond to the reversible behavior rather both reduction and oxidation peaks corresponded to independent charge transfer processes. This was further confirmed through recording the cyclic voltammograms at different scan rates.

For a reversible redox couple, the increasing scan rate increases the current without changing the E_p value while an irreversible oxidation or reduction process will suffer a peak shift towards more positive or negative value respectively upon increasing scan rate [19]. It was observed that the increasing scan rates from 100 mV/s to 700 mV/s, the oxidation peaks suffered a positive shift in peak potential and an increase in current. This showed that raising the scan rate increases the oxidation, so, it was a fast oxidative process. On the other hand, the response of reduction peak was interesting as it suffered a shift in peak potential towards positive value (negative shift in reduction peak) along with an increase in peak current. This revealed that the reduction process was facilitated by the increase in oxidation process. Therefore, it can be inferred that the reduction process followed oxidation process.

This was further confirmed by reversing the direction of scan where neither oxidation peak nor reduction peak was recorded (Fig. 5 **inset**).

Table 1
Alkaline phosphatase inhibitory activity of synthesized compounds **9a-j**.

Compounds	Alkaline Phosphatase IC_{50} ± SEM (μM)	Free radical % scavenging (100 μg/mL)
9a	2.374 ± 0.071	10.13 ± 0.01
9b	1.233 ± 0.036	10.00 ± 0.03
9c	1.233 ± 0.036	4.00 ± 0.02
9d	5.012 ± 0.091	8.32 ± 0.08
9e	4.844 ± 0.145	12.35 ± 0.6
9f	4.801 ± 0.310	35.50 ± 1.06
9g	**3.765 ± 0.112**	**2.5 ± 0.065**
9h	0.420 ± 0.012	13.67 ± 0.31
9i	1.793 ± 0.053	15.0 ± 0.35
9j	8.348 ± 0.250	12.45 ± 0.27
KH_2PO_4	2.80 ± 0.065	–
Vitamin C	–	96.91 ± 3.0

Values are presented as Mean ± SEM Standard error of mean.

Table 2
Kinetic analysis of compound **9h.**

Entry	Concentration (μM)	$1/V_{max}$ (ΔA/Min)	K_m mM	K_i (μM)	Inhibition type
1	0.00	200.00	1.0952	0.360	
2	0.100	363.63	1.0952	0.360	Non-competitive
3	0.200	436.36	1.0952	0.360	
4	0.400	500.00	1.0952	0.360	

1/Vmax is the inverse of reaction velocities, Km is the Michaelis-Menten constant, Ki is the inhibition constant.

Thus, the reduction process was following irreversible oxidation process and was not coupled with it reversibly. Further, the increasing scan rate did not reduce the peak current of any peak, eradicating the association of any coupled chemical reaction with oxidation process. Moreover, the two successive scan at each scan rate resulted in reproduction of both voltammograms (data not shown here) revealing that couple chemical reaction was not associated with any of charge transfer process. Therefore, the E_oE_r (electron transfer oxidation followed by electron transfer reduction) was suggested as charge transfer mechanism.

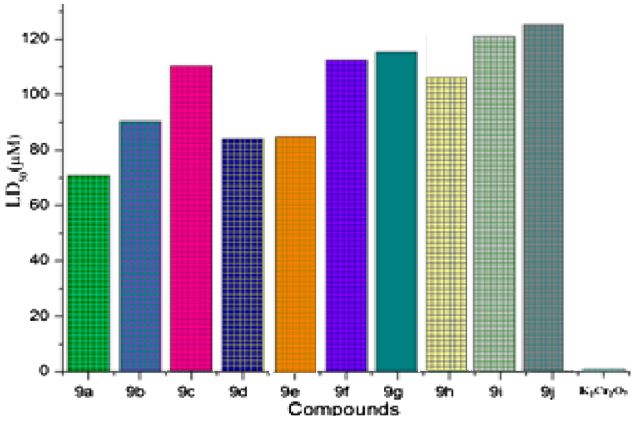

Fig. 2. The graphical depiction of LD_{50} (μM) values of synthesized compounds **9a-j**.

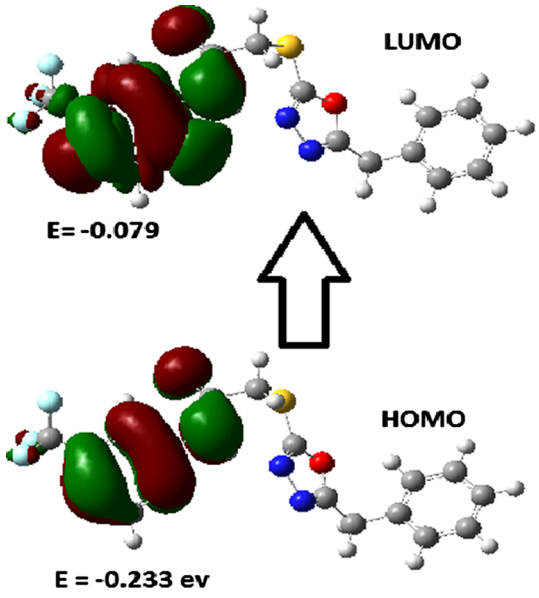

Fig. 3. HOMO and LUMO of the compounds (DFT/B3LYP/6-311G**(++)).

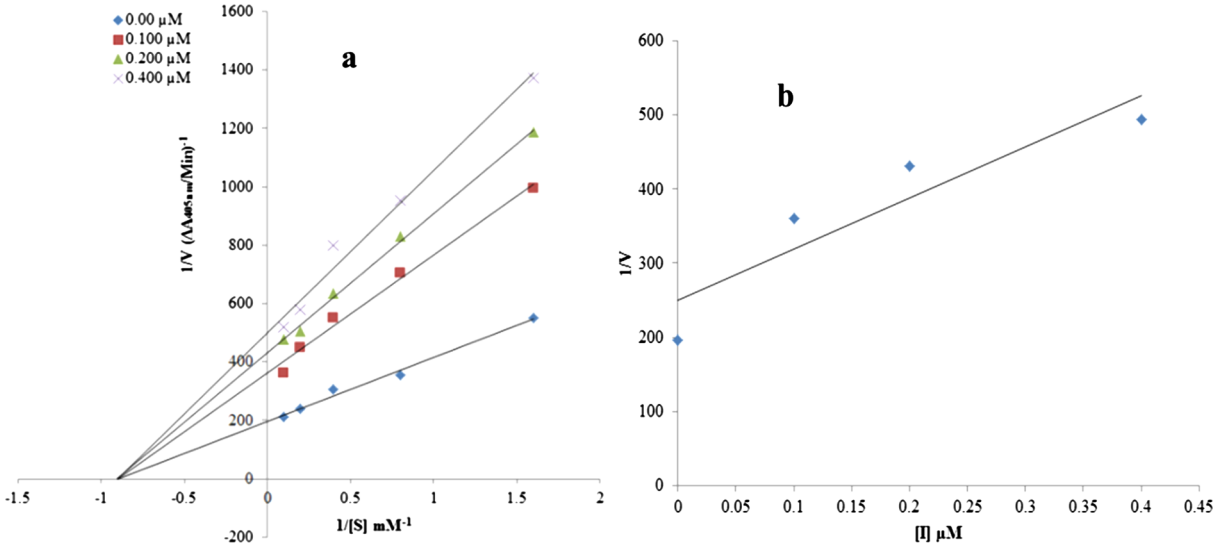

Fig. 1. (a) Lineweaver–burk plots for the inhibition of compound **9h** on Calf alkaline phosphatase; concentrations were 0.00, 0.100, 0.200 and 0.400 mM. The (b) represents the secondary plot of 1/Vmax versus concentration of compound **9h** to determine the inhibition constant (*Ki*).

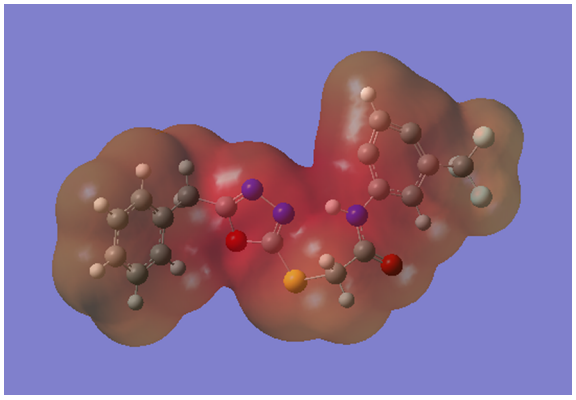

Fig. 4. The computed molecular electrostatic potential energy surface (MPES) of **9h** at DFT/B3LYP/6-311G**(++) level of theory.

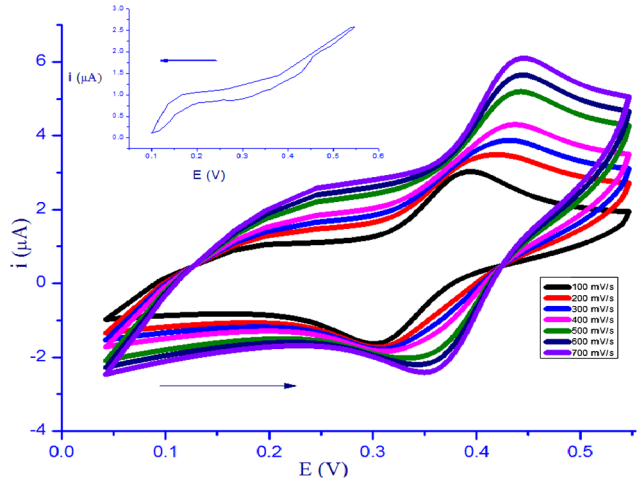

Fig. 5. Cyclic voltammograms of **9h** in 50% methanol-PBS (pH-7.4) at different scan rates vs. SEC scanned form 0 to 0.6 V. Inset: Cyclic voltammogram under same conditions scanned from 0.6 to 0 V at 100 mV/s.

2.5.2. DNA binding studies of *9h*

The UV–Vis spectrum for **9h** exhibited two peaks at 245 nm and 205 nm Fig. 6. When DNA was added to **9h**, the absorbance decreased without any shift in λ_{max}. The successive addition DNA resulted in successive decrease in absorbance which was then used to obtain formation constant through Benesi-Hildebrand equation [20]. As there was no shift in $\lambda_{max,}$ the electrostatic binding and intercalation stamped

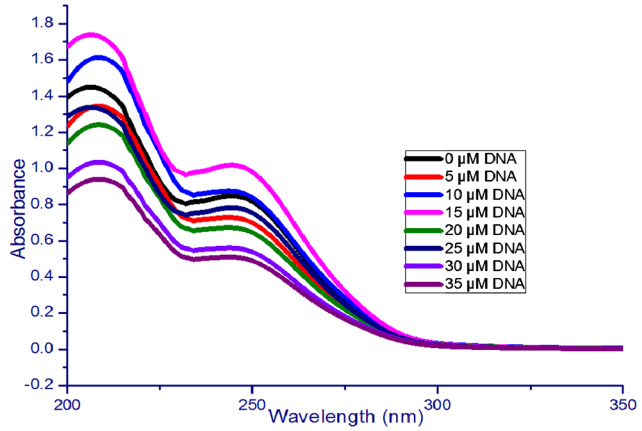

Fig. 6. UV–Vis spectra of **9h** (20 μM) in 50% methanol-PBS (pH-7.4) in the presence of different concentrations of DNA.

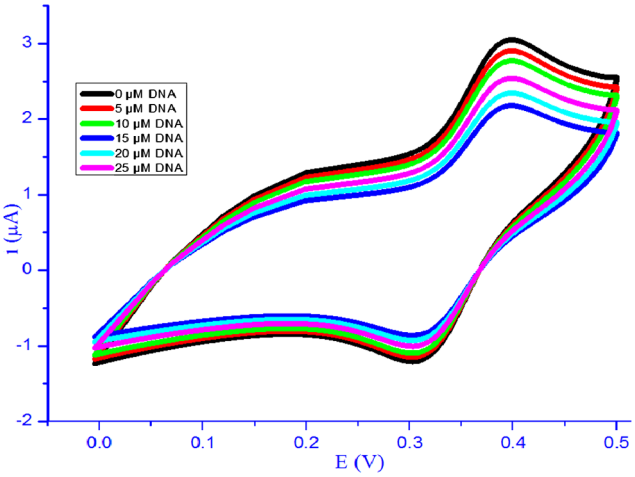

Fig. 7. Cyclic voltammograms of **9h** (30 mM) in 50% methanol-PBS (pH-7.4) at 0.1 V/s vs SCE in the presence of different concentrations of DNA.

out. Based on observed hypochromism, the groove binding was suggested for **9h**-DNA interactions.

When the DNA was added to the **9h**, the peak current decreased and the E_p did not shift for oxidation and reduction peaks. The incremental addition of DNA resulted in successive peak current decrease without effecting the position of any peak Fig. 7. The intact E_p depicts that **9h** charge transfer process was not disturbed by DNA addition, rather only diffusion was troubled. Further, the diffusion co-efficient was calculated to be 6.5×10^{-4} cm^2/s for **9h** and 0.54×10^{-4} cm^2/s for **9h**-DNA mixture which revealed the significant reduction in diffusion coefficient of **9h** through its binding to DNA. Thus, the decrease in peak current can be attributed to decrease in diffusion coefficient due to **9h**-DNA complex formation. Such cyclic voltammetric responses often stand for fitting of drug into grooves of DNA [21]. Therefore, the cyclic voltammetry confirmed the groove binding of **9h** with DNA as was indicated by UV–Vis spectroscopy.

The binding constants calculated from UV–Vis spectroscopy and cyclic voltammetry (Fig. 8) were 7.83×10^3 and 7.95×10^3 M^{-1} respectively which revealed significant strength of **9h**-DNA complex.

2.6. Molecular docking analysis

2.6.1. Binding energy evaluation of synthesized compounds

Molecular docking experiment is best approach to study the binding conformation of ligands against target protein [22,23]. For the prediction of the best conformational position within the active region of targeted protein, all the synthesized ligands (**9a-j**) were docked against ALP. All the generated docked complexes were analyzed on the basis of minimum energy values (kcal/mol) and hydrogen/hydrophobic interactions. From the docking results it was concluded that all the ligands possessed good binding energy values and interestingly no huge energy difference was being observed among all docked complexes. The docking results predicted compound **9h** to be most active that exhibited good energy value (−7.90 kcal/mol) in comparison to other derivatives. Moreover, **9a** and **9f** also exhibited good binding energy values (−7.70 and −7.60 kcal/mol). Whereas, **9d, 9e** and **9i** possessed common energy value (−7.50 kcal/mol energy). The other compounds also presents significance energy values against receptor molecule. Although, the basic chemical nucleus of all the synthesized compounds was same, therefore most of ligands showed good efficient energy values (Fig. 9).

2.6.2. Binding pocket analysis of *9j* against alkaline phosphatase

9h-docked complex was selected based on in vitro (IC_{50}) and docking results, to deeply recognize the binding interaction behavior of

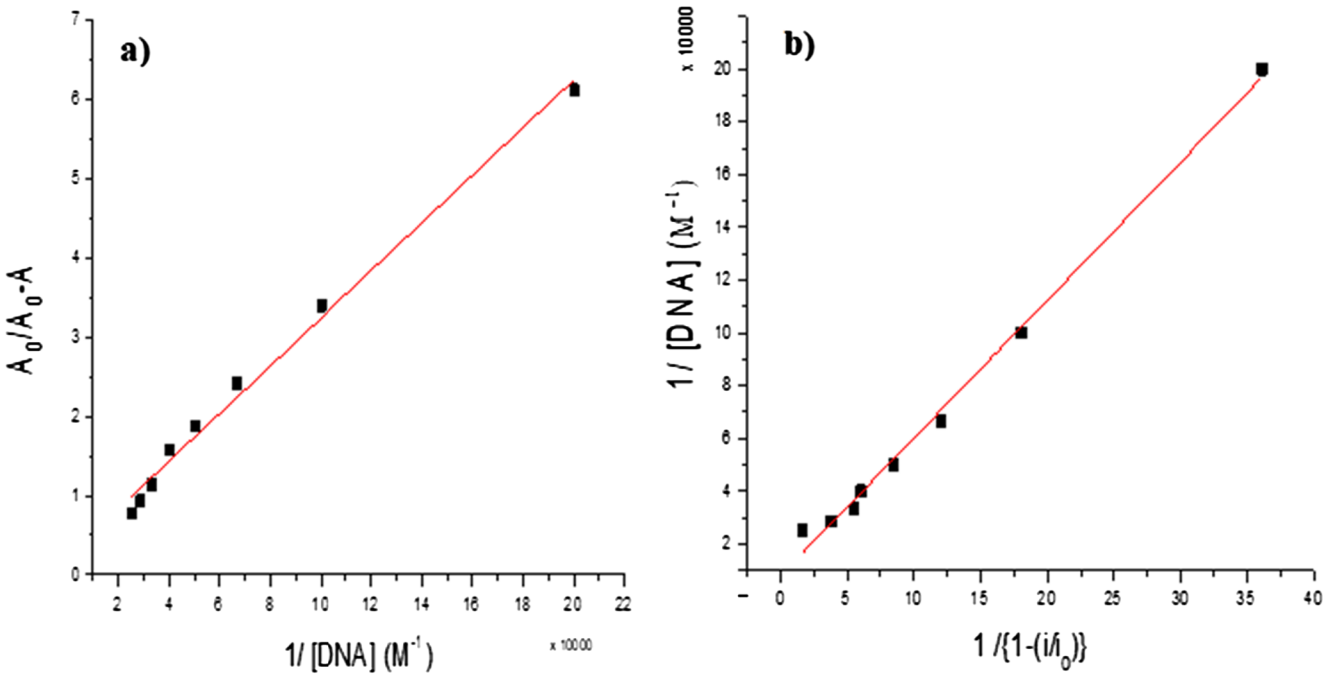

Fig. 8. (a) UV–visible data (b) Cyclic voltammetric data of **9h** plots for calculation of k_f.

ligand against target protein. Docking analysis depicted that compound **9h** was actively confined within active binding region of receptor molecule (Fig. 10**A, B**). The phenolic ring structure showed their intrusion within the inner part of binding pocket, whereas, the bulky triflorometh yl moiety remain outside in the opening region of binding pocket. These triflorometh yl may cause a little steric hindrance which may restrict this part to gain entry inside the binding pocket.

2.6.3. Hydrogen binding analysis

In detail, the binding analysis study showed that two hydrogen bonds were observed in **9h**-docking complex. The carbonyl oxygen atom of **9h** forms hydrogen bond with Thr 431 and fluorine incorporated moiety also showed hydrogen bond with Val89 having bond lengths 2.57 and 2.95 Å, respectively (Fig. 11**A, B**). Research data also ensured the importance of these residues in bonding with other ALP inhibitors which strengthen our docking result [24,25]. The comparative binding energy and SAR analysis showed the significance of **9h** compound and may consider as potent inhibitor by targeting ALP.

3. Conclusions

Substituted phenyl[(5-benzyl-1,3,4-oxadiazol-2-yl)sulfanyl]acetates/acetamides **9a-j** were efficiently synthesized in good yields. The alkaline phosphatise inhibitory kinetics revealed that compound **9h** displayed most potent activity with IC_{50} value 0.420 ± 0.012 µM while IC_{50} value of standard (KH_2PO_4) was 2.80 µM and showing non-competitive mode of binding with enzyme. Molecular docking studies performed against alkaline phosphatase enzyme (1EW2) showed that **9h** exhibited excellent binding affinity having binding energy value (−7.90 kcal/mol) compared to other derivatives. The brine shrimp viability assay results proved that derivative **9h** was non-toxic at concentration used for enzyme assay. The lead compound **9h** showed LD_{50}

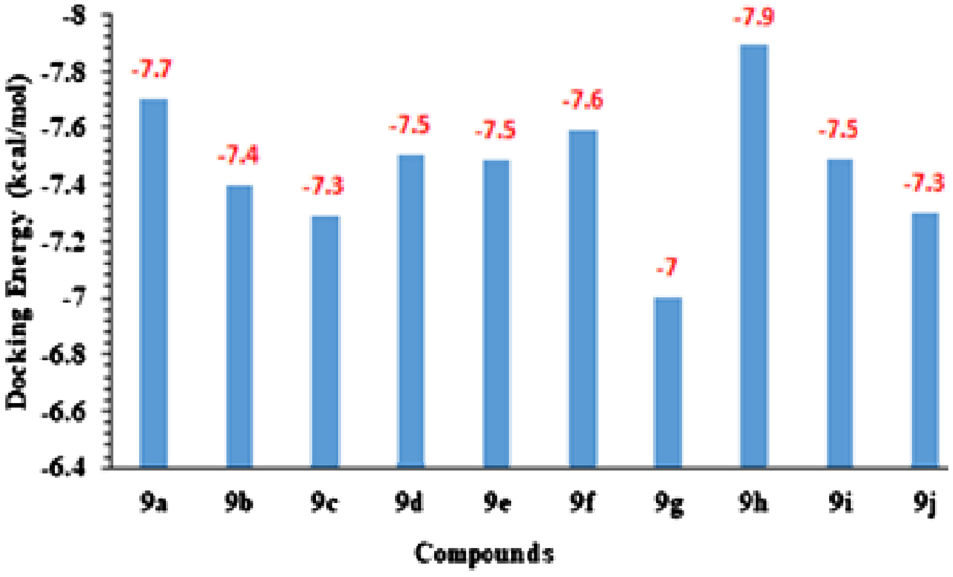

Fig. 9. The graphical depiction of docking energy values of synthesized compounds **9a-j**.

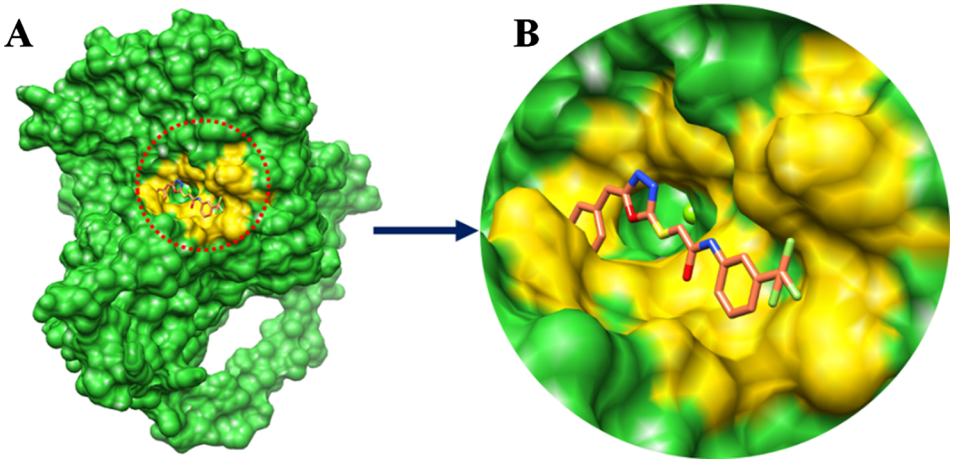

Fig. 10. (A, B) Binding pocket depiction of **9h** within active region of target protein.

106.71 μM while the standard potassium dichromate showed LD_{50} 0.891 μM. The DNA binding interactions of the synthesized compound **9h** was also determined experimentally by spectrophotometric and electrochemical methods. The compound **9h** was found to bind with grooves of DNA as depicted by both UV–Vis spectroscopy and cyclic voltammetry with binding constant values 7.83×10^3 and $7.95 \times 10^3\ M^{-1}$ respectively revealing significant strength of **9h**-DNA complex. As dry lab and wet lab results concise each other it was concluded that synthesized compounds, especially compound **9h** may serve as lead compound to design most potent inhibitors of human ALP.

4. Materials and methods

4.1. Chemistry

The necessary chemicals and reagents were purchased from Sigma Aldrich Company and no further purification was needed. Melting point was determined through Digital Gallenkamp (SANYO) apparatus. Furthermore, FTIR spectrum of synthesized compounds was determined through Perkin Elmer spectrophotometer. ^1H NMR and ^{13}C NMR spectra were determined in $CDCl_3$ solutions at 300 MHz via Brukner AM-300 spectrophotometer. Elemental Analysis (C, H, N) were carried out on a Flash 2000 series elemental analyzer with TCD detector system and results are with ± 0.3%.

4.1.1. Synthesis of 5-benzyl-1,3,4-oxadiazole-2-thiol

Phenyl acetic acid **1** was being esterified by refluxing methanol (20 mL), Phenyl acetic acid (5 g) and few drops of sulphuric acid in a round bottom flask for 6 h. Phenyl acetic acid hydrazide**3** was being synthesized by refluxing Phenyl acetic ester **2** (2 mmol), ethanol (20 mL) and hydrazine mono-hydrate (3 mmol) for 6 h. TLC technique was being used to determine the progress of the reaction and the reaction mixture was concentrated under low pressure in order to obtain solid phenylacetohydrazide **3** and was also being recrystallized in ethanol [26]. 5-benzyl-1,3,4-oxadiazole-2-thiol **4** was synthesized by mixing phenylacetohydrazide **3** (10 mmol), KOH (6 mmol) and dry ethanol (20 mL) in a round bottom flask. Then CS_2 was added in reaction mixture in portions (20 mmol) and was being refluxed for 12 h. Completion of reaction was as confirmed through TLC, was concentrated under the reduced pressure and was then acidified with HCl

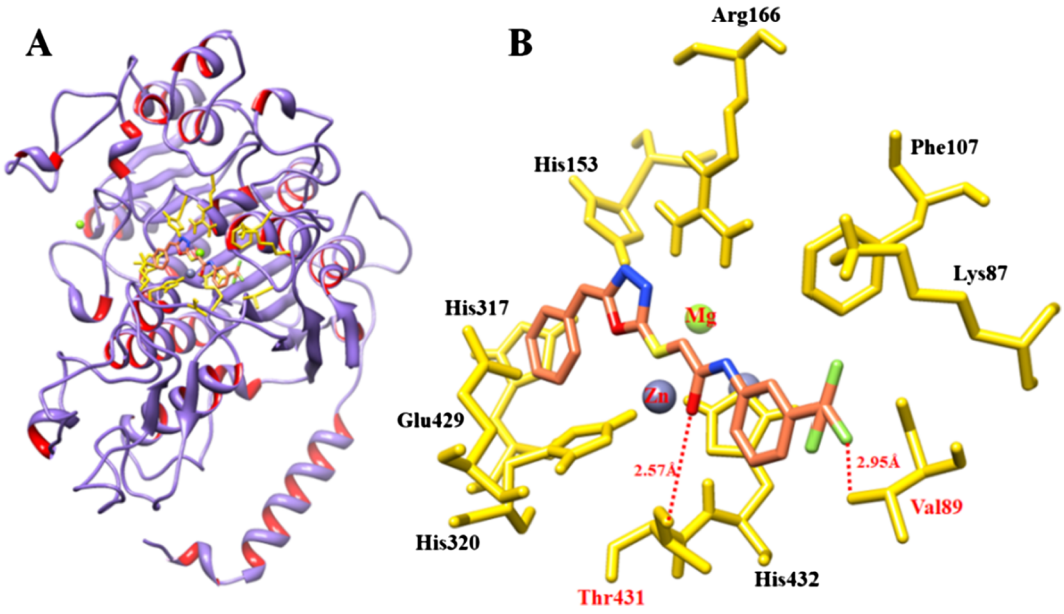

Fig. 11. (A) Docking interactions of **9h** with alkaline phosphate. (B) the basic skeleton of **9h** is represented in brown, whereas, their functional moieties are justified in red, blue, yellow and light green colours. The interacted residues are represented in yellow. Amino acids involved in hydrogen bonding are labelled with red colour, having distances mentioned in angstrom (Å).

to afford oxadiazole **4** as yellow ppts. Ethanol was being used for recrystalization of oxadiazole **4**; Yield: 79.9%; **FTIR** (KBr, ν_{max} cm^{-1}): 2951 (sp^3 C—H stretch), 1617 (C═N), 1511 (C═C aromatic), 1231 (C—O).

*4.1.2. Synthesis of phenyl 2-chloroacetate derivatives **6a-f***

Phenyl 2-chloroacetate derivatives **6a-f** were synthesized by reacting **5a-f** (2 mmol) with chloroacetylchloride (2 mmol), triethyl amine (2 mmol) and dichloromethane as solvent (20 mL), the reaction mixture was continued for stirring up to 6 h. Finally, under the maintained low pressure the reaction mixture was being concentrated and product was extracted in ethylacetate.

*4.1.2.1. Synthesis of 2-chloro-N-phenylacetamide derivatives **8a-d**.* 2-chloro-N-phenylacetamide derivatives **8a-d** were synthesized by reacting **7a-d** (2 mmol) with chloroacetylchloride (2 mmol), (triethyl amine 2 mmol) and dichloromethane (20 mL), the reaction mixture was kept on stirring for 6 h. The reaction mixture was being concentrated on low pressure and product was extracted in ethyl acetate.

*4.1.3. Synthesis of 1,3,4 oxadiazole derivatives **9a-f***

5-benzyl-1,3,4-oxadiazole-2-thiol **4** (5 mmol), acetone (20 mL) and K_2CO_3 (10 mmol) was added in a round bottom flask followed by continuous stirring. Furthermore, chloroacetyl chloride derivatives **6a-f** (6 mmol) were added in above reaction mixture and heated under reflux for 12 h. The progress of the reaction was being monitored through TLC. After the completion of reaction; the obtained reaction mixture was placed under low pressure to get concentrated solid oxadiazole derivatives **9a-f** which was purified by applying column chromatography [27].

*4.1.4. Synthesis of 1,3,4 oxadiazole derivatives **9g-j***

5-benzyl-1,3,4-oxadiazole-2-thiol **4** (5 mmol), acetone (20 mL) and K_2CO_3 (10 mmol) was added in a round bottom flask followed by continuous stirring. Furthermore, chloroacetyl chloride derivatives **8a-d** (6 mmol) were added in above reaction mixture and heated under reflux for 12 h. The progress of the reaction was monitored through TLC. After the completion of reaction the obtained reaction mixture was placed under low pressure to get concentrated solid oxadiazole derivatives **9g-j** which was purified by applying column chromatography [28,29].

*4.1.4.1. Phenyl 2-((5-benzyl-1,3,4-oxadiazol-2-yl)thio)acetate **9a**.* Yield: 68.5% FTIR (KBr, ν_{max} cm^{-1}): 3211 (sec. amide NH), 2988 (sp^2 C—H stretch), 2943 (sp^3 C—H stretch), 1690 (C═O), 1592 (C═N), 1489 (C═C aromatic), 1224 (C—O). **^{1}H NMR** ($CDCl_3$, δ ppm): 7.39 (1H, m, H-15), 7.34 (2H, m, H-13,17), 7.24 (2H, m, H-14,16), 7.11 (2H, m, H-2,4), 7.07 (2H, m, H-1,5), 6.81 (1H, m, H-3), 4.08 (2H, s, H-10) 3.07 (2H, s, H-7); **^{13}C NMR** ($CDCl_3$, δ ppm): 167.7 (C-11), 166.5 (C-9), 163.5 (C-8), 155.8 (C-12), 130.1 (C-13,17), 129.5 (C-15), 124.4 (C-3), 121.4 (C-14,16), 120.3 (C-6), 116.0 (C-1,5), 115.4 (C-2,4), 34.2 (C-10), 30.9 (C-7); Anal Calcd For $C_{17}H_{14}N_2O_3S$: C, 62.57; H, 4.29; N, 8.58 Found C, 62.50; H, 4.23; N, 8.51.

*4.1.4.2. 2-methoxyphenyl 2-((5-benzyl-1,3,4-oxadiazol-2-yl)thio)acetate **9b**.* Yield: 75.7%; FTIR (KBr, ν_{max} cm^{-1}): 2954 (sp^2 C—H stretch), 2837 (sp^3 C—H stretch), 1713 (C═O), 1611 (C═C aromatic), 1511 (C═N). **^{1}H NMR** ($CDCl_3$, δ ppm): 7.26 (2H, d, *J = 8.4*H-1,5), 7.12 (3H, m, H-2,3,4), 6.96 (2H, m, H-15,16), 6.96 (1H, d, *J = 7.2*H-14), 6.77 (1H, d, *J = 8.3*H-3), 4.30 (2H, s, H-10), 4.11 (2H, s, H-7) 3.91 (3H, s, H-18). **^{13}C NMR** ($CDCl_3$, δ ppm):167.2 (C-11), 155.2 (C-9), 150.7 (C-8), 130.1 (C-14,17), 129.6 (C-12), 127.3 (C-13),125.2 (C-15) 122.5 (C-16), 120.6 (C-2,4), 115.8 (C-6), 110.9 (C-1,5), 112.4 (C-3), 105.4 (C-18), 33.9 (C-10), 31.0 (C-7); Anal Calcd For $C_{18}H_{16}N_2O_4S$: C, 60.67; H, 4.49; N, 7.86 Found C, 60.61; H, 4.43; N, 7.79.

*4.1.4.3. 2-isopropyl-5-methylphenyl 2-((5-benzyl-1,3,4-oxadiazol-2-yl)thio)acetate **9c**.* Yield: 70.2%; m.p. 220 °C FTIR (KBr, ν_{max} cm^{-1}): 2989 (sp^2 C—H stretch), 2944 (sp^3 CH stretch), 1760 (C═O), 1686 (C═C aromatic), 1488 (C═N) ^{1}H NMR ($CDCl_3$, δ ppm): 7.83 (1H, s, H-17), 7.33 (3H, m, H-2,3,4), 7.06 (2H, d, *J = 8.8*H-1,5), 6.70 (1H, d, *J = 6.8*H-14), 6.28 (1H, d, *J = 7.2*H-15), 4.18 (2H, s, H-10), 4.11 (3H, s, H-21), 4.02 (2H, s, H-7), 3.60 (1H, m, H-18), 1.18 (6H, d, *J = 3.3*H-19,20) **NMR** ($CDCl_3$, δ ppm): 168.2 (C-11), 166.5 (C-8),164.4 (C-9), 138.8 (C-12), 137.6 (C-17), 136.0 (C-15), 133.9 (C-2,4), 128.8 (C-1,5), 127.8 (C-13) 126.6 (C-6), 122.9 (C-3), 119.9 (C-16), 118.8 (C-14), 39.2 (C-10), 31.2 (C-7), 30.8 (C-18), 26.2 (C-19,20), 23.4 (C-21); Anal Calcd For $C_{21}H_{22}N_2O_3S$: C, 65.96; H, 5.75; N, 7.32 Found C, 65.88; H, 5.69; N, 7.26.

*4.1.4.4. 4-allyl-2-methoxyphenyl 2-((5-benzyl-1,3,4-oxadiazol-2-yl)thio) acetate **9d**.* Yield: 80.2%; m.p. 74 °C FTIR (KBr, ν_{max} cm^{-1}): 2936 (sp^2 C—H stretch), 2944 (sp^3 CH stretch), 1755 (C═O), 1637 (C═C aromatic) 1507 (C═N). **^{1}H NMR** ($CDCl_3$, δ ppm): 7.34 (1H, s, H-14), 7.33 (1H, d, *J = 7.7*H-16), 7.32 (1H, d, *J = 7.2*H-17), 6.95 (2H, d, *J = 8.4*H-1,5), 6.75 (3H, m, H-2,3,4), 5.92 (1H, m, H-20), 5.18 (2H, m, H-21),4.29 (2H,d, *J = 15*H-19), 4.21 (2H, s, H-10), 3.97 (3H, s, H-18), 3.19 (2H, s, H-7). **^{13}C NMR** ($CDCl_3$, δ ppm): 167.3 (C-11), 165.8 (C-9), 161.2 (C-8), 139.7 (C-12), 137.5 (C-13), 133.7 (C-14), 130.5 (C-1,5),129.7 (C-17), 129.0 (C-6), 128.8 (C-15), 127.7 (C-3), 124.2 (C-2,4), 122.8 (C-20), 114.4 (C-16), 108.8 (C-21), 56.1 (C-18) 40.2 (C-19), 30.9 (C-10), 21.1 (C-7); Anal Calcd For $C_{21}H_{20}N_2O_4S$: C, 63.63; H, 5.05; N, 7.07 Found C, 63.57; H, 4.98; N, 7.01.

*4.1.4.5. 4-formyl-2-methoxyphenyl 2-((5-benzyl-1,3,4-oxadiazol-2-yl) thio)acetate **9e**.* Yield: 85.5 FTIR (KBr, ν_{max} cm^{-1}): 2983 (sp^2 C—H stretch), 2942 (sp^3 C—H stretch), 1692 (C═O), 1588 (C═C aromatic), 1507 (C═N). **^{1}H NMR** ($CDCl_3$, δ ppm): 9.75 (1H, s H-19), 7.38 (1H, s, H-14), 7.36 (1H, d, *J = 7.4*H-16), 7.32 (1H, d, *J = 7.2*H-17), 7.30 (3H, m, H-2,3,4), 6.95 (2H, d, *J = 8.4*H-1,5), 4.11 (2H, s, H-10), 4.06 (2H, s, H-7), 3.89 (3H, s, H-18). **^{13}C NMR** ($CDCl_3$, δ ppm): 191.3 (C-19), 157.8 (C-11), 151.8 (C-9), 147.2 (C-8), 139.7 (C-12), 136.5 (C-13) 129.7 (C-14), 129.5 (C-17), 129.0 (C-16), 128.8 (C-15), 128.5 (C-2,4), 127.7 (C-1,5), 114 (C-3), 108.8 (C-6), 56.1 (C-18), 33.9 (C-10), 31.7 (C-7); Anal Calcd For $C_{19}H_{16}N_2O_5S$: C, 59.37; H, 4.16; N, 7.29 Found C, 59.31; H, 4.09; N, 7.22.

*4.1.4.6. Benzo[d][1,3]dioxol-5-yl 2-((5-benzyl-1,3,4-oxadiazol-2-yl)thio) acetate **9f**.* Yield: 84.5%; FTIR (KBr, ν_{max} cm^{-1}): 2954 (sp^2 C—H stretch), 2893 (sp^3 C—H stretch), 1755 (C═O), 1636 (C═C aromatic), 1580 (C═N). ^{1}H NMR ($CDCl_3$, δ ppm): 7.46 (2H, m, H-13,17), 7.44 (1H, d, *J = 7.3*H-16), 7.36 (3H, m, H-2,3,4), 7.04 (2H, d, *J = 9.0*H-1,5), 6.02 (2H, s, H-18), 4.05 (2H, s, H-10), 3.98 (2H, s, H-7). **^{13}C NMR** ($CDCl_3$, δ ppm): 167.2 (C-11), 165.5 (C-9), 165.4 (C-8), 149.7 (C-15), 147.4 (C-14), 137.6 (C-12), 133.0 (C-14), 129.0 (C-16), 129.0 (C-13), 128.8 (C-17), 127.8 (C-3), 120.6 (C-2,4), 110.9 (C-6), 105.4 (C-18), 38.2 (C-10), 33.4 (C-7); Anal Calcd For $C_{18}H_{14}N_2O_5S$: C, 58.37; H, 3.78; N, 7.56 Found C, 58.30; H, 3.70; N, 7.47.

*4.1.4.7. 2-((5-benzyl-1,3,4-oxadiazol-2-yl)thio)-N-phenylacetamide **9g**.* Yield: 75.7%; m.p. 142 °C FTIR (KBr, ν_{max} cm^{-1}): 3064 (sp^2 C—H stretch), 2968 (sp^3 C—H stretch), 1661 (C═O amide), 1597 (C═C aromatic), 1495 (C═N). ^{1}H NMR ($CDCl_3$, δ ppm): 9.17 (1H, NH), 7.39 (2H, d, *J = 7.2*H 13,17), 7.35 (2H, d, *J = 8.7*H-1,5), 7.32 (3H, m, H-14,15,16), 6.87 (3H, m, H-2,3,4), 4.20 (2H, s, H-10), 3.98 (2H, s, H-7). **^{13}C NMR** ($CDCl_3$, δ ppm): 167.2 (C-11), 165.5 (C-8), 165.4 (C-9),137.0 (C-12), 133.0 (C-6), 129.5 (C-13,17), 128.5 (C-2,4), 127.6 (C-1,5), 126.7 (C-14,16), 124.6 (C-15), 119.9.7 (C-3), 36.2 (C-10), 31.8 (C-7); Anal Calcd For $C_{17}H_{15}N_3O_2S$: C, 62.76; H, 4.61; N, 12.92 Found C, 62.69; H, 4.55; N, 12.85.

*4.1.4.8. 2-((5-benzyl-1,3,4-oxadiazol-2-yl)thio)-N-(3-(trifluoromethyl) phenyl)acetamide **9h**.* Yield: 78.3%; m.p. 75 °C FTIR (KBr, ν_{max} cm^{-1}): 3218 (sec. amide NH), 3031 (sp^2 C—H stretch), 2911 (sp^3 C—H stretch), 1686 (C═O amide), 1660 (C═C aromatic), 1601 (C═N). ^{1}H NMR ($CDCl_3$, δ ppm): 9.20 (1H, s, NH), 7.93 (2H, s, H-13), 7.29 (1H, d, *J = 7.8*H-15), 7.18 (1H, m, H-16), 7.15 (1H, d, *J = 8.2*H-17), 7.14 (2H, d, *J = 7.4*H-1,5), 6.95 (3H, m, H-2,3,4), 3.89 (2H, s, H-10), 3.41 (2H, s, H-7). ^{13}C NMR ($CDCl_3$, δ ppm): 169.2 (C-11), 166.6 (C-8),165.4 (C-9), 137.7 (C-14), 134.4 (C-13), 129.3 (C-15), 129.0 (C-16), 129.4 (C-12), 129.1 (C-17), 128.9 (C-2,4), 127.3 (C-1,5), 127.3 (C-3), 126.7 (C-6), 118.5 (C-18), 39.1 (C-10), 32.8 (C-7); Anal Calcd For $C_{18}H_{14}N_2O_2SF_3$: C, 54.96; H, 3.56; N, 10.68 Found C, 54.90; H, 3.49; N, 10.61.

*4.1.4.9. 2-((5-benzyl-1,3,4-oxadiazol-2-yl)thio)-N-(4-bromophenyl) acetamide **9i**.* Yield: 72.5%; m.p. 248 °C **FTIR** (KBr, ν_{max} cm^{-1}): 3362 (sec. amide NH), 3137 (sp^2 C—H stretch), 2976 (sp^3 C—H stretch) 1677 (C═O amide), 1608 (C═C aromatic), 1556 (C═N). **^{1}H NMR** ($CDCl_3$, δ ppm): 9.24 (1H, NH), 7.33 (2H, d, *J = 7.5 Hz*, H-14,16), 7.29 (2H, d, *J = 7.2 Hz*, H-13,17), 7.33 (2H, m, H-2,4), 7.32 (2H, m, H-1,5), 6.72 (1H, m, H-3), 3.99 (2H, s, H-10), 3.29 (2H, s, H-7). **^{13}C NMR** ($CDCl_3$, δ ppm): 167.2 (C-11), 165.5 (C-8), 165.4 (C-9), 137.6 (C-12), 133.1 (C-14,16), 129.0 (C-13,17), 128.0 (C-1,5), 127.8 (C-2,4), 124.8 (C-3), 119.6 (C-15), 119.9 (C-6), 36.2 (C-10), 31.8 (C-7); Anal Calcd For $C_{17}H_{14}N_3O_2SBr$: C, 50.49; H, 3.46; N, 10.39 Found C, 50.43; H, 3.39; N, 10.32.

*4.1.4.10. 2-((5-benzyl-1,3,4-oxadiazol-2-yl)thio)-N-(4-chlorophenyl) acetamide **9j**.* Yield: 88.3%; FTIR (KBr, ν_{max} cm^{-1}): 3250 (sec. amide NH), 3197 (sp^2 C—H stretch), 2967 (sp^3 C—H stretch), 1674 (C═O amide), 1647 (C═C aromatic), 1587 (C═N). ^{1}H NMR ($CDCl_3$, δ ppm): 9.24 (1H, s, NH), 7.33 (2H, d, *J = 7.5*H-14,16), 7.28 (2H, d, *J = 8.2*H-13,17), 7.20 (2H, m, H-1,5), 7.19 (2H, d, *J = 7.2*H-2,4), 6.78 (1H, m, H-3), 3.99 (2H, s, H-10), 3.29 (2H, s, H-7). **^{13}C NMR** ($CDCl_3$, δ ppm): 167.3 (C-11), 165.6 (C-8),165.4 (C-9), 136.2 (C-12), 132.9 (C-14,16), 129.8 (C-15), 129.5 (C-6), 129.2 (C-13,17), 128.8 (C-1,5), 129.8 (C-3), 129.2 (C-2,4), 36.1 (C-10), 31.8 (C-7); Anal Calcd For $C_{17}H_{14}N_3O_2S$: C, 56.74; H, 3.89; N, 11.68 Found C, 56.68; H, 3.83; 11.61.

4.2. Alkaline phosphatase inhibition assay

Previously described method was being used to measure the activity of calf IALP by spectrophotometric assay [30]. The reaction mixture was pre-incubated for 10 min by adding 5 μL of CIALP (0.025 U/mL), 50 mMTris-HCl buffer (5 mM $MgCl_2$, 0.1 mM $ZnCl_2$ pH 9.5), the compound (0.1 mM with final DMSO 1% (v/v) and mixture. After this 10 μL of substrate para nitrophenylphosphate disodium salt was being added to initiate the reaction. At 37 °C the assay mixture was incubated again for 30 min. OPT MAX, Tunable USA, 96-well micro plate reader was being used to check the change in absorbance of released *p*-nitrophenolate and was being monitored at 405 nm. Experiments were repeated in triplicate manner and potassium dihydrogen phosphate was used as a reference inhibitor of CIALP.

4.3. Kinetic studies

The most potent inhibitor **9h** was being selected for determination of the mechanism of enzyme inhibition on the basis of IC_{50} value. We took inhibitor concentrations in the range of 0.0, 0.100, 0.200 and 0.400 μM. Similarly the substrate p-NPP was taken in concentrations of 10, 5, 2.5, 1.25 and 0.625 mM. Same conditions were being maintained for pre-incubation time as described in ALP inhibition assay. Enzyme was being added at per minute's interval and maximal initial velocities were also determined from initial linear portion of absorbance up to 10 min. The enzyme inhibition type was assayed by Lineweaver-Burk plot. The graph was being plotted as **1/V** (inverse of velocities) versus**1/[S]** (inverse of substrate concentration) mM^{-1}. The secondary plot of 1/V versus concentration of inhibitor was being determined by EI dissociation constant *Ki*.

4.4. Free radical scavenging assay

2,2-diphenyl-1 picrylhydrazyl (DPPH) assay was being used to determine radical scavenging activity using already reported method with slight modifications [31,32]. 100 μL of DPPH (150 μM), 20 μL test compounds was used as assay solution and the volume was attuned to 200 μL in each well with DMSO. At room temperature the reaction mixture was then incubated for 30 min. For radical scavenging Vitamin C (Ascorbic acid) was used as a reference inhibitor. The assay measurements were carried out by using $OPTI_{Max}$, Tunable micro plate reader at 517 nm. The percent inhibition caused by the presence of tested inhibitors was being calculated by comparing the reaction rates. Each concentration was analyzed in three independent experiments run in triplicate.

4.5. Cytotoxicity evaluation using brine shrimp assay

4.5.1. Culturing and harvesting of Artemiasalina

Two uneven compartments were being made by rectangular dish with a plastic divider with several holes in which Artemiasalina cysts were incubated for hatching. The container was filled with 3.3% solution of artificial sea water. The dry yeast sprinkled into the larger darkened compartment while the smaller compartment was illuminated with light and temperature was maintained at 28 °C. Artificial light and aeration was being used for incubation and after 24 h, hatched A. salina cysts were transferred to fresh artificial seawater. It was again incubated for 24 h. From the lighted compartment the phototropic nauplii were being collected using pipette.

4.5.2. Brine shrimps assay

Pasteur pipette was being used for counting macroscopically A. salinanauplii (20) against a lighted background. It was then transferred into each sample vial and the solutions were diluted with brine solution to 5 mL with test compound. A drop of dry yeast suspension was added to each vial as food and the vials were maintained under light. The surviving nauplii were counted with the aid of a magnifying glass after 24 h. The mean mortality at the three dose levels for compound was determined and repeated in triplicate. Potassium dichromate was used as reference standard. After 24 the LD_{50} were calculated by Probit analysis.

4.6. Molecular docking study

4.6.1. Retrieval of alkaline phosphate structure from PDB

The 3D structure of ALP from human placenta was being accessed from PDB having PDBID 1EW2. UCSF Chimera 1.10.1 tool was being used to minimize the selected target protein structure [33]. Stereochemical properties of ALP were generated by Protparam tool [34]. Discovery Studio 4.1 Client tool was being used for hydrophobicity and Ramachandran plot of ALP [35]. Online server VADAR 1.8 was being used for prediction of protein architecture and statistical percentage values of receptor proteins helices, beta-sheets, coils and turn [36].

4.6.2. Designing of ligands and molecular docking

ACD/Chem Sketch tool were used to sketch and draw synthesized ligands and were being minimized by UCSF Chimera 1.10.1 and then were access in mol format. Furthermore, UCSF Chimera 1.10.1 tool was used for energy minimization of each ligand separately. Default parameters such as steepest descent steps 100 with step size 0.02 (Å), conjugate gradient steps 100 with step size 0.02 (Å) and update interval was fixed at 10. Finally, to obtain the good structure conformation, Gasteiger charges were added using Dock Prep in ligand structure [37]. PyRx virtual screening tool with AutoDock VINA Wizard approach was

employed for molecular docking experiment on all the synthesized ligands against ALP [38]. Active region of the targeted protein was being selected for better conformational position by using grid box center values of (center X = 43.3, center Y = 23.1612 and center Z = 9.1269) and size values were adjusted as (X = 65.56, Y = 71.79, and Z = 64.64). The ligands **9a-j** were docked separately against ALP with default exhaustiveness value = 8. The predicted docked complexes were evaluated on the basis of lowest binding energy (Kcal/mol) values. Discovery Studio (2.1.0) and UCSF Chimera 1.10.1 tool were used for 3D graphical depictions of all the docked complexes.

4.7. DFT calculations

The geometric and electronic computations were performed at DFT/B3LYP/6-311G**(++)basis sets [39] for DFT/B3LYP/6-311G level optimized geometry using the Gaussian 03/Gauss view 09 software.

4.8. DNA binding studies

The 0.1 M NaH_2PO_4 and 0.1 M Na_2HPO_4were mixed to prepare sodium phosphate buffer of pH-7.4 which also acted as supporting electrolyte in electrochemistry. Calf thymus DNA was extracted through standard Falcon method. The DNA sample with absorbance ratio (A_{260}/A_{280}) > 1.8 was considered sufficiently pure to be stored at −4 °C for DNA interaction experiments and its molarity was established from its absorbance at 260 nm against $\varepsilon = 6600\,M^{-1}\,cm^{-1}$ [40]. All the reagents used were of analytical grade and every experiment was performed in triplicate. A 3 mM stock solution of the **9h** in 50% methanol-phosphate buffer mixture was diluted to required concentrations. The **9h** (20 μM) solution was titrated against variable concentration (5, 10…35 μM) of DNA and differential spectra was analyzed through Benesi-Hildebrand relation for K_b calculation. The cyclic voltammograms of **9h** (30 mM in 50% methanol-phosphate buffer) titration with DNA was recorded at 0.1 V/s vs. SCE at 310 K. The current change was exploited through the following equation [41].

$$\frac{1}{[DNA]} = \left[\frac{K_f(1-A)}{\left\{1-\frac{i}{i_0}\right\}}\right] - K_f \quad (1)$$

Declaration of Competing Interest

The authors declare no conflict of interest.

References

[1] S. Kishore, A. Khanna, Z. Zhang, J. Hui, P.J. Balwierz, M. Stefan, C. Beach, R.D. Nicholls, M. Zavolan, S. Stamm, The snoRNA MBII-52 (SNORD 115) is processed into smaller RNAs and regulates alternative splicing, Hum. Mol. Genet. 19 (7) (2010) 1153–1164, https://doi.org/10.1093/hmg/ddp585.

[2] D. Patel, M. Bolland, Z. Nisa, F. Al-Abuwsi, M. Singh, A. Horne, I. Reid, C. McGhee, Incidence of ocular side effects with intravenous zoledronate: secondary analysis of a randomized controlled trial, Osteopor. Int. 26 (2) (2015) 499–503, https://doi.org/10.1007/s00198-014-2872-5.

[3] H. Nisa, A.N. Kamili, I.A. Nawchoo, S. Shafi, N. Shameem, S.A. Bandh, Fungal endophytes as prolific source of phytochemicals and other bioactive natural products: a review, Microb. Pathog. 82 (2015) 50–59, https://doi.org/10.1016/j.micpath.2015.04.001.

[4] N.K.N.A. Zawawi, M. Taha, N. Ahmat, A. Wadood, N.H. Ismail, F. Rahim, M. Ali, N. Abdullah, K.M. Khan, Novel 2,5-disubtituted-1,3,4-oxadiazoles with benzimidazole backbone: a new class of β-glucuronidase inhibitors and in silico studies, Bioorg. Med. Chem. 23 (13) (2015) 3119–3125, https://doi.org/10.1016/j.bmc.2015.04.081.

[5] G. Ramaprasad, B. Kalluraya, B.S. Kumar, R.K. Hunnur, Synthesis and biological property of some novel 1,3,4-oxadiazoles, Eur. J. Med. Chem. 45 (10) (2010) 4587–4593, https://doi.org/10.1016/j.ejmech.2010.07.021.

[6] I. Khan, M. Hanif, M.T. Hussain, A.A. Khan, M.A.S. Aslam, N.H. Rama, J. Iqbal, Synthesis, acetylcholinesterase and alkaline phosphatase inhibition of some new 1,2,4-triazole and 1,3,4-thiadiazole derivatives, Aust. J. Chem. 65 (10) (2012) 1413–1419, https://doi.org/10.1071/CH12134.

[7] M.-H. Le Du, J.L. Millán, Structural evidence of functional divergence in human alkaline phosphatases, J. Biol. Chem. 277 (51) (2002) 49808–49814, https://doi.org/10.1074/jbc.M207394200.

[8] L. Zhang, M. Balcerzak, J. Radisson, C. Thouverey, S. Pikula, G. Azzar, R. Buchet, Phosphodiesterase activity of alkaline phosphatase in ATP-initiated Ca^{2+} and phosphate deposition in isolated chicken matrix vesicles, J. Biol. Chem. 280 (44) (2005) 37289–37296, https://doi.org/10.1074/jbc.M504260200.

[9] M. Al-Rashida, S.A. Ejaz, S. Ali, A. Shaukat, M. Hamayoun, M. Ahmed, J. Iqbal, Diary sulfonamides and their bioisosters as dual inhibitors of alkaline phosphatase and carbonic anhydrase: structure activity relationship and molecular modeling studies, Bioorg. Med. Chem. 23 (10) (2015) 2435–3244, https://doi.org/10.1016/j.bmc.2015.03.054.

[10] F. Sacco, L. Perfetto, L. Castagnoli, G. Cesareni, The human phosphatase interactome: An intricate family portrait, FEBS Lett. 586 (17) (2012) 2732–2739, https://doi.org/10.1677/joe.1.05723.

[11] J. Roy, M.S. Cyert, Cracking the phosphatase code: docking interactions determine substrate specificity, Sci. Signal. 2 (100) (2009) re9-re9, https://doi.org/10.1016/j.febslet.2012.05.008.

[12] I.P. Maly, E. Eppler, M. Müller-Gerbl, High metabolic activity of tissue-nonspecific alkaline phosphatase not only in young but also in adult bone as demonstrated using a new histochemical detection protocol, Gen. Comp. Endocrinol. (2017), https://doi.org/10.1016/j.ygcen.2017.05.008.

[13] S. Sidique, R. Ardecky, Y. Su, S. Narisawa, B. Brown, J.L. Millán, E. Sergienko, N.D. Cosford, Design and synthesis of pyrazole derivatives as potent and selective inhibitors of tissue-nonspecific alkaline phosphatase (TNAP), Bioorg. Med. Chem. Lett. 19 (1) (2009) 222–225, https://doi.org/10.1016/j.ygcen.2017.05.008.

[14] S. Hassan, S.A. Ejaz, A. Saeed, M. Shehzad, S.U. Khan, J. Lecka, J. Sévigny, G. Shabir, J. Iqbal, 4-Aminopyridine based amide derivatives as dual inhibitors of tissue non-specific alkaline phosphatase and ecto-5′-nucleotidase with potential anticancer activity, Bioorg. Chem. 76 (2018) 237–248, https://doi.org/10.1016/j.bioorg.2017.11.013.

[15] Mariia Miliutina, Syeda Abida Ejaz, Viktor O. Iaroshenko, Alexander Villinger, Jamshed Iqbal, Peter Langer, Synthesis of 3,3′-carbonyl-bis(chromones) and their activity as mammalian alkaline phosphatase inhibitors, Org. Biomol. Chem. 14 (2) (2016) 495–502 http://xlink.rsc.org/?DOI=C5OB01350Jhttps://doi.org/10.1039/C5OB01350J.

[16] Mari S. Karthikeyan, Bantwal S. Holla, Synthesis, antiinflammatory and antimicrobial activities of some 2,4-dichloro-5-fluorophenyl substituted arylidene-triazolothiazolidinones, Monatsh. Chem. 139 (6) (2008) 691–696 http://link.springer.com/10.1007/s00706-007-0794-zhttps://doi.org/10.1007/s00706-007-0794-z.

[17] Z. Chen, W. Xu, K. Liu, S. Yang, H. Fan, P.S. Bhadury, Y. Zhang, Synthesis and antiviral activity of 5–(4–chlorophenyl)-1, 3, 4-thiadiazole sulfonamides, Molecules 15 (12) (2010) 9046–9056, https://doi.org/10.3390/molecules15129046.

[18] N. Foroughifar, A. Mobinikhaledi, S. Ebrahimi, M.A.B. Fard, H. Moghanian, A simple and efficient procedure for synthesis of optically active 1, 2, 4-triazolo-[3, 4-b]-1, 3, 4-thiadiazole derivatives containing l-amino acid moieties, J. Chin. Chem. Soc. 56 (5) (2009) 1043–1047, https://doi.org/10.1002/jccs.200900151.

[19] G.A. Mabbott, An introduction to cyclic voltammetry, J. Chem. Educ. 60 (1983) 697, https://doi.org/10.1021/ed060p697.

[20] Niranjan A. Panat, Beena G. Singh, Dharmendra K. Maurya, Santosh K. Sandur, Saroj S. Ghaskadbi, Troxerutin, a natural flavonoid binds to DNA minor groove and enhances cancer cell killing in response to radiation, Chem. Biol. Interact. 251 (2016) 34–44 https://linkinghub.elsevier.com/retrieve/pii/S0009279716300941https://doi.org/10.1016/j.cbi.2016.03.024.

[21] M. Sirajuddin, S. Ali, A. Badshah, Drug–DNA interactions and their study by UV–Visible, fluorescence spectroscopies and cyclic voltametry, J. Photochem. Photobiol. B: Biol. 124 (2013) 1–19, https://doi.org/10.1016/j.jphotobiol.2013.03.013.

[22] M. Hassan, Z. Ashraf, Q. Abbas, H. Raza, S.-Y. Seo, Exploration of novel human tyrosinase inhibitors by molecular modeling, docking and simulation studies, Interdiscip. Sci. Comput. Life Sci. 10 (1) (2018) 68–80, https://doi.org/10.1016/j.bioorg.2017.11.013.

[23] A. Ibrar, S. Zaib, I. Khan, F. Jabeen, J. Iqbal, A. Saeed, Facile and expedient access to bis-coumarin–iminothiazole hybrids by molecular hybridization approach: synthesis, molecular modelling and assessment of alkaline phosphatase inhibition, anticancer and antileishmanial potential, RSC Adv. 5 (109) (2015) 89919–89931, https://doi.org/10.1039/c5ra14900b.

[24] M. Hassan, H. Raza, M.A. Abbasi, A.A. Moustafa, S.-Y. Seo, The exploration of novel Alzheimer's therapeutic agents from the pool of FDA approved medicines using drug repositioning, enzyme inhibition and kinetic mechanism approaches, Biomed. Pharmacother. 109 (2019) 2513–2526, https://doi.org/10.1016/j.biopha.2018.11.115.

[25] M. Hassan, S. Shahzadi, S.Y. Seo, H. Alashwal, N. Zaki, A.A. Moustafa, Molecular docking and dynamic simulation of AZD3293 and solanezumab effects against BACE1 to treat Alzheimer's disease, Front. Comput. Neurosci. 12 (2018), https://doi.org/10.3389/fncom.2018.00034.

[26] H. He, W. Wang, Y. Zhou, Q. Xia, Y. Ren, J. Feng, H. Peng, H. He, L. Feng, Rational design, synthesis and biological evaluation of 1,3,4-oxadiazole pyrimidine derivatives as novel pyruvate dehydrogenase complex E1 inhibitors, Bioorg. Med. Chem. 24 (8) (2016) 1879–1888, https://doi.org/10.1016/j.bmc.2016.03.011.

[27] V.R. Pidugu, N.S. Yarla, S.R. Pedada, A.M. Kalle, A.K. Satya, Design and synthesis of novel HDAC8 inhibitory 2, 5-disubstituted-1,3,4-oxadiazoles containing glycine and alanine hybrids with anti cancer activity, Bioorg. Med. Chem. 24 (21) (2016) 5611–5617, https://doi.org/10.1016/j.bmc.2016.09.022.

[28] L. Chen, P. Wang, Z. Li, L. Zhou, Z. Wu, B. Song, S. Yang, Antiviral and antibacterial activities of N-(4-substituted phenyl) acetamide derivatives bearing 1, 3, 4-

oxadiazole moiety, Chin. J. Chem. 34 (12) (2016) 1236–1244, https://doi.org/10.1002/cjoc.201600501.
[29] H. Shah, New 1,3,4- oxadiazoles as an antitubercular agents, Ind. J. 8 (12) (2012) 447–449.
[30] J. Iqbal, An enzyme immobilized microassay in capillary electrophoresis for characterization and inhibition studies of alkaline phosphatases, Anal. Biochem. 414 (2) (2011) 226–231, https://doi.org/10.1016/j.bmc.2016.09.022.
[31] S.M. Reddy, J. Mudgal, P. Bansal, S. Vasanthraju, K. Srinivasan, C.M. Rao, N.G. Kutty, Antioxidant, anti-inflammatory and anti-hyperglycaemic activities of heterocyclic homoprostanoid derivatives, Bioorg. Med. Chem. 19 (1) (2011) 384–392, https://doi.org/10.1016/j.bmc.2015.06.068.
[32] Z. Ashraf, M. Rafiq, S.-Y. Seo, M.M. Babar, Synthesis, kinetic mechanism and docking studies of vanillin derivatives as inhibitors of mushroom tyrosinase, Bioorg. Med. Chem. 23 (17) (2015) 5870–5880, https://doi.org/10.1016/j.bmc. 2015.06.068.
[33] E.F. Pettersen, T.D. Goddard, C.C. Huang, G.S. Couch, D.M. Greenblatt, E.C. Meng, T.E. Ferrin, UCSF Chimera visualization system for exploratory research and analysis, J. Comput. Chem. 25 (13) (2004) 1605–1612, https://doi.org/10.1016/j.bmc.2015.06.068.
[34] E. Gasteiger, C. Hoogland, A. Gattiker, M.R. Wilkins, R.D. Appel, A. Bairoch, Protein identification and analysis tools on the ExPASy server, The Proteomics Protocols Handbook, Springer, 2005, pp. 571–607, , https://doi.org/10.1385/1-59259-890-0:571.
[35] R. Qamar, A. Saeed, F.A. Larik, Q. Abbas, M. Hassan, H. Raza, S.Y. Seo, Novel 1, 3-oxazine-tetrazole hybrids as mushroom tyrosinase inhibitors and free radical scavengers: synthesis, kinetic mechanism, and molecular docking studies, Chem. Biol. Drug Des. 93 (2) (2019) 123–131, https://doi.org/10.1016/j.bmc.2015.06.068.
[36] L. Willard, A. Ranjan, H. Zhang, H. Monzavi, R.F. Boyko, B.D. Sykes, D.S. Wishart, VADAR: a web server for quantitative evaluation of protein structure quality, Nucl. Acids Res 31 (13) (2003) 3316–3319, https://doi.org/10.1093/nar/gkg565.
[37] A. Saeed, G. Saddique, P.A. Channar, F.A. Larik, Q. Abbas, M. Hassan, H. Raza, T.A. Fattah, S.-Y. Seo, Synthesis of sulfadiazinyl acyl/aryl thiourea derivatives as calf intestinal alkaline phosphatase inhibitors, pharmacokinetic properties, lead optimization, Lineweaver-Burk plot evaluation and binding analysis, Bioorg. Med. Chem. 26 (12) (2018) 3707–3715, https://doi.org/10.1016/j.bioorg.2017.11.013.
[38] S. Dallakyan, A.J. Olson, Small-molecule library screening by docking with PyRx, Chemical Biology, Springer, 2015, pp. 243–250, , https://doi.org/10.1007/978-1-4939-2269-719.
[39] F. Javed, S. Ali, S. Shahzadi, N. Khalid, S. Tabassum, I. Khan, S.K. Sharma, K. Qanungo, Synthesis, spectroscopy, semi-empirical and biological activities of organotin (IV) complexes with o-isopropyl carbonodithioic acid, J. Chin. Chem. Soc. 62 (8) (2015) 728–738, https://doi.org/10.1002/jccs.201500235.
[40] F. Perveen, N. Arshad, R. Qureshi, J. Nowsherwan, A. Sultan, B. Nosheen, H. Rafique, Electrochemical, spectroscopic and theoretical monitoring of anthracyclines' interactions with DNA and ascorbic acid by adopting two routes: Cancer cell line studies, PLoS ONE 13 (10) (2018) e0205764, https://doi.org/10.1371/journal.pone.0205764.
[41] E. Jabeen, N.K. Janjua, S. Hameed, β-Cyclodextrin assisted solubilization of Cu and Cr complexes of flavonoids in aqueous medium: a DNA-interaction study, Spectrochim. Acta Part A Mol. Biomol. Spectrosc. 128 (2014) 191–196, https://doi.org/10.1016/j.saa.2014.02.132.